applied sciences

MDPI

Article

ISAC-Enabled NR-V2X PC5 Sidelink with Direct-Path Cancellation for Vehicular Bistatic Sensing

Moin Ali, Sung Won Kim and Ali Nauman *

Department of Computer Science and Engineering, Yeungnam University, Gyeongsan 38541, Republic of Korea; moinali@yu.ac.kr (M.A.); swon@yu.ac.kr (S.W.K.)
* Correspondence: anauman@ynu.ac.kr

Abstract

Reliable vehicle-to-everything (V2X) communication increasingly requires roadside infrastructure to perceive surrounding traffic while sharing limited radio resources with safety-critical data exchange. Integrated sensing and communication (ISAC) offers a potential means of using existing sidelink transmissions for both functions, but strong direct-path reception, incomplete waveform references, and synchronization errors challenge practical bistatic sensing. This paper investigates the reuse of NR-V2X PC5 sidelink waveforms for simulated roadside-unit (RSU) bistatic sensing. The communication branch generates PSCCH/PSSCH signals, whereas the sensing branch evaluates a synchronized two-channel reference/surveillance receiver; passive acquisition of arbitrary transmitted payloads and physical receiver calibration are not demonstrated. Established single-reference least-squares (LS) cancellation is benchmarked against tuned normalized LMS, a restricted three-template ECA-like receiver, and a no-cancellation diagnostic using matched simulated observations. For 30 independent noise seeds with 50 packets per seed, the pooled nominal excess-path root-mean-square errors are 0.5458, 0.5457, 1.9806, and 27.0201 m, respectively. The LS mean seed-level RMSE is 0.5458 m (95% Student-*t* confidence interval 0.5437–0.5478 m). A 49-condition speed–reflection sweep gives pooled errors of 0.4058–0.6429 m. A separate eleven-point communication experiment reports an aggregate 96.64% SL-SCH transport-block success rate, not end-to-end packet delivery ratio. An isolated-path fractional-delay experiment and reference-channel sensitivity tests further characterize estimator assumptions and synchronization limitations. These findings establish simulation-level waveform-reuse feasibility under the stated receiver model; interference, physical RSU operation, and traffic generalization remain open.

Keywords: NR-V2X; PC5 sidelink; integrated sensing and communication; ISAC; RSU; bistatic sensing; direct-path cancellation; V2X

Check for updates

Academic Editor: Christos Bouras

Received: 1 October 2026
Revised: 5 November 2026
Accepted: 18 November 2026
Published: 22 November 2026

Copyright: © 2026 by the authors. Licensee MDPI, Basel, Switzerland. This article is an open access article distributed under the terms and conditions of the Creative Commons Attribution (CC BY) license.

1. Introduction

Vehicle-to-everything (V2X) communication has become one of the main enablers for cooperative and automated driving. Early vehicular networks mainly focused on the periodic exchange of safety messages among nearby vehicles. However, modern connected mobility services require more than simple awareness exchange. Advanced driving, cooperative perception, automated maneuvering, platooning, vulnerable road-user protection, and infrastructure-assisted safety services require vehicles and roadside units to share timely information while also understanding the surrounding radio and traffic environment [1–3]. For this reason, V2X systems are moving toward a joint communication and perception

model where the wireless signal is not only used to deliver data, but can also provide sensing information about nearby objects and moving targets.

The Third Generation Partnership Project (3GPP) has standardized LTE V2X and NR-V2X to support direct and network-assisted vehicular communication. In NR-V2X, the PC5 sidelink interface enables direct vehicle-to-vehicle, vehicle-to-infrastructure, and vehicle-to-pedestrian communication without requiring every packet to pass through the cellular network [4–7]. The NR sidelink physical layer uses channels such as PSCCH and PSSCH to carry control and data information, and the resource structure is flexible enough to support multiple service requirements [8–11]. These characteristics make NR-V2X PC5 a suitable candidate for safety-critical direct communication. At the same time, the transmitted sidelink waveform is an available radio-frequency signal in the road environment, and this creates an opportunity to reuse the same waveform for sensing.

Integrated sensing and communication (ISAC) has recently gained strong attention for 5G-Advanced and 6G systems because it allows communication and sensing functions to share spectrum, hardware, waveform resources, and signal-processing chains [12–15]. In the IMT-2030 vision, ISAC is considered as one of the key usage scenarios for future wireless systems [16,17]. 3GPP has also started formal studies on ISAC service requirements and NR-based ISAC design [18,19]. These activities show that future wireless networks are expected to support not only data transmission, but also target detection, range estimation, motion tracking, environmental awareness, and infrastructure-assisted perception.

A substantial body of sensing work already examines cellular waveforms, passive bistatic receivers, and NR-V2X sidelink sensing [20–24]. The operating assumptions and measurement tasks differ, however, and a matched evaluation of a reference-aided PC5 sidelink transmitter-to-RSU bistatic configuration remains useful. In a road scenario, a vehicle may already transmit a PC5 sidelink packet to a neighboring vehicle. The same transmitted signal may also reach a roadside unit (RSU) through a direct Tx-VUE-to-RSU path and through a reflected path from a moving vehicle target. This creates a bistatic sensing opportunity without requiring an additional sensing-only transmission. However, this reuse is not straightforward. The direct path from the transmitting vehicle to the RSU is usually much stronger than the target-reflected path. If the RSU directly correlates the received signal with the transmitted waveform, the reflected component can be hidden by the direct-path peak and its sidelobes. Therefore, direct-path suppression is necessary before reliable reflected-path estimation.

Motivated by this issue, we examine a reference-aided simulation model for NR-V2X PC5 bistatic sensing: a Tx-VUE communicates with an Rx-VUE over PSCCH/PSSCH resources, while a synchronized RSU reference/surveillance receiver uses a measured reference to suppress the dominant direct path and estimate target excess-path delay. The transmitted waveform in the MATLAB R2025b experiment is known to its waveform generator; in the passive-reference variant, noisy reference-channel measurements are supplied to the sensing processing chain. This controlled experiment does not establish acquisition of unknown SCI/PSSCH data, deployable synchronization, or hardware cancellation. Conventional LS projection, normalized LMS and ECA-style subspace cancellation are established signal-processing methods; the present contribution is their matched evaluation in the defined PC5 waveform-reuse scenario, not invention of a new cancellation algorithm.

The contributions are:

- An explicit PC5 communication–bistatic sensing architecture, including a conditional synchronized RSU reference-channel assumption and its deployment limitations.
- A packet-index/sample-index bistatic signal model with target-motion phase/Doppler, fractional-delay refinement, common search-window definitions and reported reference-quality sensitivity.

- Matched four-receiver cancellation and error comparisons with 30 independent noise seeds, a 49-condition speed/reflection study, separate communication and isolated-path delay experiments, and explicit numerical uncertainty.
- An explicit comparison of communication, bistatic sensing, and isolated-path estimation experiments that avoids pooling incompatible observations, and a quantitative assessment of simulator-specific performance limits.

The rest of this paper is organized as follows. Section 2 reviews related work on NR-V2X sidelink communication, ISAC, and vehicular sensing. Section 3 presents the proposed ISAC-enabled NR-V2X PC5 sidelink framework. Section 4 describes the simulation setup and evaluation methodology. Section 5 discusses the numerical results. Finally, Section 6 concludes the paper and outlines future research directions.

2. Related Work

This section reviews the main research directions related to the proposed work: NR-V2X PC5 sidelink communication, integrated sensing and communication, and vehicular ISAC.

2.1. NR-V2X PC5 Sidelink Communication

NR-V2X was introduced to support advanced vehicular services that require direct, reliable, and low-latency communication among vehicles, roadside infrastructure, pedestrians, and cellular networks. Different from conventional cellular communication, the PC5 sidelink interface enables direct communication between nearby V2X devices without forcing every packet to pass through the base station or the core network. This feature is important for safety-related applications because local vehicular information must often be exchanged within a short time and under rapidly changing mobility conditions [4,5,25].

The NR-V2X sidelink physical layer relies on several physical channels and procedures. The physical sidelink control channel (PSCCH) carries sidelink control information, while the physical sidelink shared channel (PSSCH) carries the sidelink data payload and related control information. The overall sidelink transmission and reception procedure depends on the configured resource pool, modulation and coding configuration, channel estimation, decoding, and HARQ-related operation [8–11]. Castañeda Garcia et al. provided a detailed tutorial on 5G NR-V2X communication, including the sidelink design, physical-layer structure, and use-case requirements [6]. Harounabadi et al. discussed NR sidelink standardization in 3GPP Release 16 and beyond [7]. Other works mainly focus on communication reliability, latency, resource allocation, and sidelink performance [26–29]. However, they do not consider how the same NR-V2X PC5 waveform can be reused for bistatic roadside sensing.

2.2. Integrated Sensing and Communication

Integrated sensing and communication has become an important research direction for 5G-Advanced and future 6G systems. The main idea of ISAC is to allow communication and sensing functions to share spectrum, hardware, waveform resources, and signal-processing modules. Instead of treating radar sensing and wireless communication as two independent systems, ISAC attempts to jointly design or reuse radio signals for both information transfer and environmental awareness [12–14]. ITU-R has identified ISAC as one of the important usage scenarios for IMT-2030 and beyond [16], while 3GPP has also initiated studies on ISAC service requirements and NR-based ISAC operation [18,19].

Existing ISAC surveys and frameworks have discussed waveform design, sensing metrics, communication-sensing tradeoffs, signal processing, and standardization challenges [15,17,30,31]. These works provide a broad foundation for ISAC research, but the specific case of NR-V2X PC5 sidelink waveform reuse for RSU-assisted bistatic sensing

remains less explored. In particular, the strong direct path between the transmitting vehicle and the RSU can dominate the weaker target-reflected path, which creates a practical sensing problem that must be addressed before reliable bistatic estimation can be achieved.

2.3. ISAC for Vehicular and Roadside Sensing

Vehicular ISAC is especially promising because connected vehicles and roadside units naturally operate in dynamic environments where both communication and perception are required. A vehicle may transmit communication signals to nearby vehicles, while those same signals may interact with moving vehicles, road objects, and roadside infrastructure. This makes vehicular networks suitable for bistatic and cooperative sensing, where one node transmits and another node observes the direct and reflected signal components.

Prior vehicular sensing research covers both the limits of NR-V2X sidelink sensing and opportunistic passive radar. Du et al. considered predictive beamforming in V2I ISAC [32], while Salami et al. investigated 5G-NR radio-frequency sensing [33]. More directly, Giovannetti et al. derived NR-V2X sidelink positioning bounds and explored multi-user interference [21]; Decarli et al. characterized communication–sensing tradeoffs for beyond-5G NR-V2X sidelink [22]. Their studies establish that the sidelink sensing problem has previously been considered and that interference and allocation choices matter.

Classical passive bistatic radar has long treated the dominant illuminator and clutter as disturbances. Colone et al. developed multistage projection-based suppression and detection, including evaluation using measured passive-radar data [20]. Nataraja et al. examined NR-based bistatic vehicular sensing using base-station transmissions, NR reference signals and high-resolution delay–Doppler processing with channel measurements [23]. Wypich and Zielinski experimentally evaluated 5G-NR OFDM passive sensing using reference, control and user data, including practical reference recovery [24]. These results should not be described as absent or reproduced here. Table 1 identifies the distinct role and limitations of our conditional PC5 RSU simulation.

Table 1. Representative passive-bistatic and NR-V2X sensing studies compared with the present work.

Study/Waveform	Sensing Focus	Difference from the Present Study
Colone et al. [20]; non-PC5 illuminator	Multistage projection cancellation; measured passive-radar evaluation	Establishes prior interference cancellation; no NR-V2X PC5 waveform experiment
Giovannetti et al. [21]; NR-V2X sidelink	Device-free target-positioning bounds under interference	Performance bounds; not a matched RSU direct-path cancellation receiver study
Decarli et al. [22]; NR-V2X sidelink	Communication–sensing tradeoffs and interference	Broad physical-layer sensitivity; not the present reference/surveillance-channel ablation
Nataraja et al. [23]; cellular 5G-NR	Opportunistic BS-to-vehicle bistatic delay–Doppler sensing	Different link direction and receiver; includes measurements not performed here
Wypich and Zielinski [24]; 5G-NR OFDM	Experimental passive radar using reference/control/user data	Practical waveform/reconstruction experiments rather than this simulated PC5 RSU pair
This work; NR-V2X PC5	Conditional dual-channel RSU sensing; LS/NLMS/ECA-like comparisons	Synchronized simulated reference required; no hardware or multi-user interference validation

2.4. Research Gap and Motivation

From the above discussion, three main research gaps can be identified. First, NR-V2X sidelink studies mainly focus on communication performance, while existing NR-V2X sensing studies have more often addressed positioning bounds or communication–sensing interference than the present reference-aided RSU cancellation experiment. Second, NR-based bistatic studies have investigated reference-signal processing and target detection, but

their transmitter/receiver arrangement and reference assumptions differ from those of the evaluated PC5 transmitter-to-RSU configuration. Third, classical passive radar already offers direct-path suppression algorithms, but their performance under the specific simulated PC5 resource, reference-channel and target-geometry configuration must be assessed rather than assumed. This study therefore evaluates established cancellation and fractional-delay methods in a defined NR-V2X PC5 sidelink bistatic sensing framework, without claiming a novel LS algorithm or demonstrating an operational passive RSU.

2.5. Positioning Against Established Passive Sensing Receivers

Direct-path least-squares projection and subtraction are standard forms of interference cancellation. Adaptive normalized least-mean-square (NLMS) methods and extensive cancellation algorithms (ECA) provide established alternatives with different convergence and model-order properties. Our matched receiver experiment contrasts these approaches under the same simulated waveform, reference model, geometry and search regions. We make no claim that the implemented single-reference LS algorithm is intrinsically superior: tuned NLMS gives essentially the same nominal RMSE, whereas the restricted three-template ECA-like configuration does worse under this particular controlled experiment. In particular, Colone et al. [20] already establish projection-based passive-radar cancellation, while Nataraja et al. [23] and Wypich and Zielinski [24] study NR-based bistatic sensing under different waveform and reference-acquisition assumptions. Comparisons should account for those architectural differences rather than only quoting RMSE. The references to 3GPP physical channels identify the underlying PC5 waveform context; they are not a claim of complete standards-conformant receiver integration.

3. Proposed ISAC-Enabled NR-V2X PC5 Sidelink Framework

This section presents the proposed ISAC-enabled NR-V2X PC5 sidelink framework. The main objective is to reuse a standard PC5 sidelink waveform for two simultaneous purposes. First, the waveform supports direct communication between a transmitting vehicle user equipment (Tx-VUE) and a receiving vehicle user equipment (Rx-VUE). Second, the same transmitted waveform is passively received by an RSU and used for bistatic sensing of a moving target vehicle.

3.1. System Overview

The considered scenario consists of four main entities: a Tx-VUE, an Rx-VUE, an RSU, and a moving target vehicle. The Tx-VUE transmits a normal NR-V2X PC5 sidelink packet using PSCCH/PSSCH resources. The Rx-VUE receives and decodes the packet through the PC5 sidelink communication channel. At the same time, the RSU receives a composite radio signal that includes a strong direct path from the Tx-VUE to the RSU and a weaker reflected path produced by the moving target vehicle. The overall system model is shown in Figure 1.

The communication branch follows the standard NR-V2X sidelink procedure and is not modified for sensing. The Tx-VUE generates the sidelink payload, prepares sidelink control information, maps the payload to the configured PC5 resources, and transmits the waveform. The Rx-VUE performs synchronization, OFDM demodulation, control-channel decoding, channel estimation, equalization, and payload recovery. The sensing branch is performed at the RSU as receiver-side processing only.

3.2. PC5 Sidelink Communication Signal Model

Let k index a transmitted PC5 packet and $n \in \{0, \ldots, N_s-1\}$ index the complex baseband samples within packet k, at sampling rate F_s. We write $x_k[n]$ for the PSCCH/PSSCH waveform and $y_{\mathrm{Rx},k}[n] = h_k[n] * x_k[n] + w_{\mathrm{Rx},k}[n]$ for the received communication waveform,

where $*$ denotes discrete-time convolution. The communication evaluation separately records SL-SCH transport-block decoding outcomes; it does not measure application-layer PDR. In the ideal-reference simulation the generated samples $x_k[n]$ are stored. In the two-channel sensitivity evaluation, a noisy, synchronized reference-channel measurement $z_k[n]$ is used; assuming such a waveform replica can be obtained passively is a modeling condition and does not demonstrate decoding unknown PSCCH/PSSCH payloads.

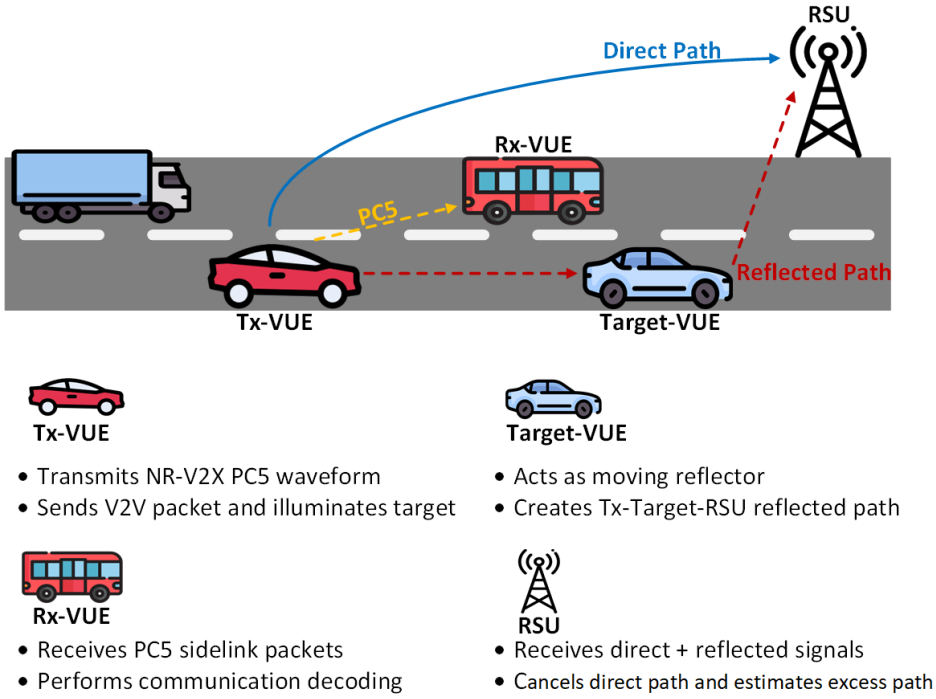


Figure 1. System model of the proposed ISAC-enabled NR-V2X PC5 sidelink framework.

3.3. RSU Bistatic Sensing and Doppler Model

For transmitter $\mathbf{p}_T$, fixed RSU $\mathbf{p}_R$, and moving target $\mathbf{p}_q(k)$, the direct and reflected bistatic lengths are

$$d_0 = \|\mathbf{p}_R - \mathbf{p}_T\|, \tag{1}$$

$$d_1(k) = \|\mathbf{p}_q(k) - \mathbf{p}_T\| + \|\mathbf{p}_R - \mathbf{p}_q(k)\|, \tag{2}$$

$$\Delta R(k) = d_1(k) - d_0, \qquad \tau_i(k) = d_i(k)/c. \tag{3}$$

The surveillance-channel baseband signal can be modeled, within a packet, as

$$y_k[n] = a_{0,k}\, x_k[n - \tau_0 F_s] + a_{1,k}\, x_k[n - \tau_1(k) F_s] e^{j2\pi f_{D,k} n/F_s} + c_k[n] + w_k[n], \tag{4}$$

where fractional shifts are implemented numerically, $c_k[n]$ is optional clutter, and $f_{D,k} \simeq -\dot{d}_1(k)/\lambda$ is the bistatic path-rate Doppler for a stationary transmitter and RSU. The carrier is 5.9 GHz and the waveform contains 15,360 samples at $F_s = 30.72$ MHz (0.5 ms); the packet snapshot spacing $\Delta T = 0.1$ s is different. The nominal trajectory is $\mathbf{p}_q(k) = [80 + 20k\Delta T, 80, 1.5]$ m, with other velocities assessed in the sensitivity sweep. The target geometry is evaluated at discrete packet times, while a Doppler phase progression models within-packet target motion. One additional stationary reflector and selected reference timing/frequency offsets are examined as stress tests; general multipath/interference are not modeled.

3.4. Reference Acquisition and Synchronization Scope

The simulated RSU uses a reference-channel observation of the direct transmitter signal alongside a surveillance-channel observation of direct and reflected arrivals. To employ $z_k[n]$ as a cancellation template, packet boundaries, common sampling-clock interpretation and the relative reference/surveillance timing must be calibrated. We do not claim an arbitrary PC5 receiver can recover unknown random PSSCH bits merely from a DM-RS signal. A DM-RS-only alternative would require its own detector and validation. Our controlled reference-quality experiment covers ideal stored-signal reference, noisy reference, a 0.25-sample inter-channel timing mismatch, and a common 100 Hz frequency offset; the latter cannot establish robustness to independent receiver oscillators.

3.5. Direct-Path Cancellation and Fractional-Delay Estimation

Write $z_{0,k}[n;\ell]$ for a numerically delayed reference template at delay ℓ/F_s. Direct delay is located by correlation within a geometry-assisted window centered at d_0 with ± 40 m extent, then refined to fractional-sample precision. The measured direct-path template $\hat{z}_{0,k}$ gives the standard one-template projection

$$\hat{a}_{0,k} = \frac{\sum_n \hat{z}^*_{0,k}[n] y_k[n]}{\sum_n |\hat{z}_{0,k}[n]|^2 + \epsilon}, \quad r_k[n] = y_k[n] - \hat{a}_{0,k}\hat{z}_{0,k}[n]. \tag{5}$$

The reflected excess-path search region is 20–220 m relative to the estimated direct path. The same geometric windows and prior information are used for all four compared receivers. A bounded fractional-delay least-squares refinement follows the initial integer-lag correlation. For delay estimates in samples $\hat{\ell}_i$, the inferred excess path is

$$\Delta\hat{R}(k) = \frac{c}{F_s}(\hat{\ell}_1(k) - \hat{\ell}_0(k)). \tag{6}$$

The sample spacing $c/F_s = 9.7589$ m is a grid interval, not a hard lower bound on single-path parameter estimation precision. The approximate bistatic path-separation scale c/B is distinct from fractional-delay estimation uncertainty; assuming $B = 20$ MHz gives 15 m, but the actual active-resource bandwidth must be identified from the allocated waveform. The separate isolated-path validation compares integer-lag, parabolic refinement, bounded LS and a conditional Cramér–Rao lower bound (CRLB). Its accuracy must not be conflated with end-to-end bistatic receiver accuracy or true multi-target resolution. The separate estimator figure therefore tests a narrower question: whether a single isolated delay can be refined between discrete sampling instants when the signal model is known. The 3.0542 m integer-lag RMSE is much larger than the 0.0509 m parabolic and 0.0114 m bounded-LS results at 20 dB, illustrating the benefit of parametric delay refinement under controlled conditions. The empirical value below the quoted 0.0130 m conditional-bound standard deviation must be treated cautiously because finite trials, model conditioning, or bound/estimator convention differences could affect direct comparison; we do not claim a violation of an applicable unbiased-estimator bound.

An excess-path-rate diagnostic may be obtained by

$$\Delta\dot{\hat{R}}(k) = \frac{\Delta\hat{R}(k) - \Delta\hat{R}(k-1)}{\Delta T}. \tag{7}$$

Finite differencing amplifies range noise and is not equivalent to an independently validated Doppler velocity estimator; the bistatic rate is a projection of target motion, not automatically its road-speed magnitude. The reflected-path simulation models Doppler-induced phase, but no independent experimental Doppler-to-velocity estimator or multi-target velocity-tracking validation is claimed.

3.6. Communication and Sensing Procedure

The communication and sensing branches are shown in Figure 2. Algorithm 1 gives the mathematical signal-flow representation of sidelink transmission, physical-channel processing, and transport-block verification. Algorithm 2 details direct-path estimation, complex LS projection, fractional-delay refinement, and bistatic excess-path conversion. The resource symbols below summarize conceptual PHY processing; unavailable SCI/MCS/RIV metadata are not inferred from the archived experiment, and full MAC compliance or payload reconstruction at a passive RSU is not claimed.

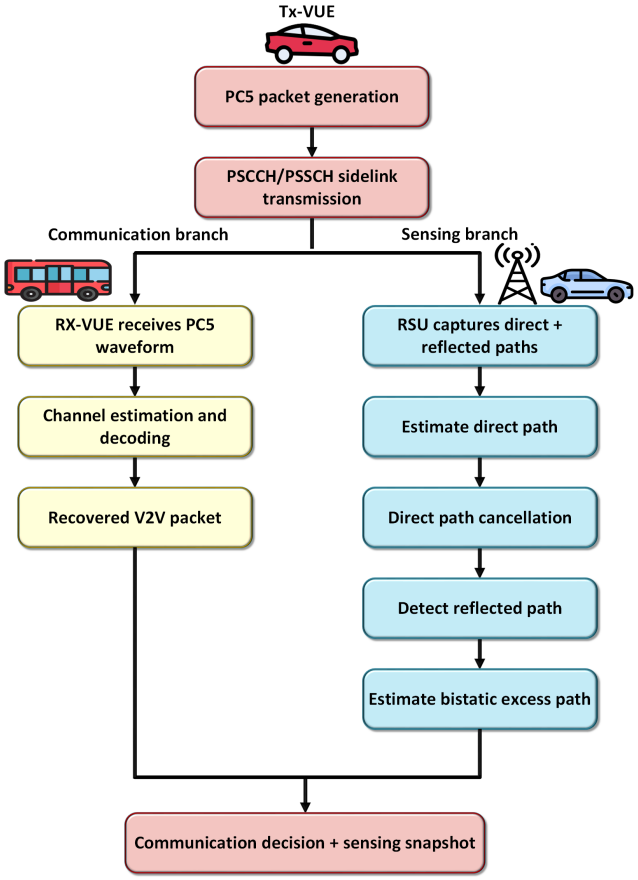


Figure 2. Procedure flow of the proposed ISAC-enabled NR-V2X PC5 sidelink framework, where a single PSCCH/PSSCH sidelink transmission is reused for both V2V communication at the Rx-VUE and RSU-based bistatic sensing through direct-path cancellation and reflected-path estimation.

Algorithm 1 NR-V2X PC5 Sidelink Communication Evaluation

procedure PC5_COMM($\mathcal{P}, C_{\mathrm{SL}}, b_k, \gamma_k$)
  $s_{1,k} \leftarrow \mathrm{SCI}_1(\mathcal{P}, C_{\mathrm{SL}})$; $s_{2,k} \leftarrow \mathrm{SCI}_2(C_{\mathrm{SL}})$
  $u_k \leftarrow \mathrm{Mux}(b_k, s_{2,k})$
  $X_k \leftarrow \mathrm{Map}_{\mathrm{PSCCH/PSSCH}}(s_{1,k}, u_k; C_{\mathrm{SL}})$
  $x_k[n] \leftarrow \mathrm{OFDMmod}(X_k)[n]$
  $y_{\mathrm{Rx,k}}[n] \leftarrow (h_{\mathrm{TDL\text{-}A30,k}} * x_k)[n] + w_k[n; \gamma_k]$
  $\widetilde{Y}_k \leftarrow \mathrm{OFDMdemod}(y_{\mathrm{Rx,k}})$
  $\hat{b}_k \leftarrow \mathrm{SL\text{-}SCHdecode}(\widetilde{Y}_k, C_{\mathrm{SL}})$
  $q_k \leftarrow \mathbf{1}\{\hat{b}_k$ passes transport-block check$\}$
  return $q_k, x_k[n]$
end procedure

Algorithm 2 Reference-Aided Direct-Path-Cancelled RSU Bistatic Sensing

procedure PC5_SENSE($y_k[n], z_k[n], F_s, \mathcal{W}_0, \mathcal{W}_1$)
  $z_k^{\mathrm{cal}}[n] \leftarrow \mathrm{Calibrate}(z_k[n])$
  $C_{0,k}(\ell) \leftarrow \left|\sum_n y_k[n] z_k^{\mathrm{cal},*}[n-\ell]\right|, \ell \in \mathcal{W}_0$
  $\ell_{0,k}^{(0)} \leftarrow \arg\max_{\ell \in \mathcal{W}_0} C_{0,k}(\ell)$
  $\hat{\ell}_{0,k} \leftarrow \mathrm{FracLS}(y_k, z_k^{\mathrm{cal}}, \ell_{0,k}^{(0)}; \mathcal{W}_0)$
  $\hat{z}_{0,k}[n] \leftarrow \mathrm{FracDelay}(z_k^{\mathrm{cal}}, \hat{\ell}_{0,k})[n]$
  $\hat{a}_{0,k} \leftarrow \dfrac{\sum_n \hat{z}_{0,k}^*[n] y_k[n]}{\sum_n |\hat{z}_{0,k}[n]|^2 + \epsilon}$
  $r_k[n] \leftarrow y_k[n] - \hat{a}_{0,k} \hat{z}_{0,k}[n]$
  $C_{1,k}(\ell) \leftarrow \left|\sum_n r_k[n] z_k^{\mathrm{cal},*}[n-\ell]\right|, \ell \in \mathcal{W}_1$
  $\ell_{1,k}^{(0)} \leftarrow \arg\max_{\ell \in \mathcal{W}_1} C_{1,k}(\ell)$
  $\hat{\ell}_{1,k} \leftarrow \mathrm{FracLS}(r_k, z_k^{\mathrm{cal}}, \ell_{1,k}^{(0)}; \mathcal{W}_1)$
  $\Delta\hat{R}(k) \leftarrow \dfrac{c}{F_s}(\hat{\ell}_{1,k} - \hat{\ell}_{0,k})$
  if $k > 0$ **then**
    $\Delta\dot{\hat{R}}(k) \leftarrow [\Delta\hat{R}(k) - \Delta\hat{R}(k-1)]/\Delta T$
  else
    $\Delta\dot{\hat{R}}(k) \leftarrow 0$
  end if
  return $\Delta\hat{R}(k), \Delta\dot{\hat{R}}(k)$
end procedure

The stored communication experiment provides block outcomes from its configured physical-layer receiver. The abstract control-channel operations in Algorithm 1 specify the intended sidelink signal flow; they should not be misread as independently verified bit-by-bit SCI reconstruction or as a measured end-to-end packet delivery process.

The lag variables $\hat{\ell}_{0,k}$ and $\hat{\ell}_{1,k}$ are measured in samples; multiplying their difference by c/F_s yields bistatic excess-path length in metres. The rate output is a finite-difference diagnostic, not an independently validated Doppler-based velocity estimate. The same geometric search regions and reference-aided assumptions apply to the compared receiver implementations. The simulation configurations for the PC5 communication and revised two-channel bistatic sensing evaluations are shown in Table 2.

Table 2. Simulation configurations for the PC5 communication and revised two-channel bistatic sensing evaluations.

Parameter	Verified Configuration
NR-V2X PC5 communication evaluation	
Physical channels	PSCCH/PSSCH; SL-SCH block decoding
Assigned bandwidth/subcarrier spacing	20 MHz/30 kHz
Waveform sampling rate/duration	30.72 MHz/0.5 ms (15,360 samples)
PSSCH modulation/target code rate	QPSK/308/1024
Transport-block size	1128 bits
Resource allocation	Two groups of 10 physical resource blocks (from stored evaluation configuration)
PSSCH DM-RS positions	Four (stored final transmission configuration)
Communication channel	TDL-A30; maximum Doppler 2700 Hz
Transmitter/receiver antennas	One/two
Receiver assumptions	Perfect channel estimation; scrambling-identity passthrough
Communication SNR/repetitions	−1.6 to 8.4 dB in 1-dB steps; 100 blocks per SNR
Communication outcome	SL-SCH transport-block success and BLER (not verified end-to-end PDR)
Revised RSU bistatic sensing evaluation	
Carrier frequency	5.9 GHz (assumed for the sensing model)
Transmit/RSU positions	[0, 0, 1.5]/[200, 0, 6] m
Moving-target initial position	[80, 80, 1.5] m

Table 2. *Cont.*

Parameter	Verified Configuration
Target movement	Positive x direction; nominal speed 20 m/s
PC5 snapshot spacing/observation	0.1 s/50 snapshots (t = 0 to 4.9 s)
RSU architecture	Simulated synchronized reference and surveillance receive channels
Nominal surveillance/reference SNR	20 dB/30 dB
Direct/reflected complex-gain magnitudes	$\|\alpha_0\| = 1$/nominal $\|\alpha_1\| = 0.35$
Direct/reflected search regions	Geometry-centered direct-path window (±40 m); reflected excess-path window 20–220 m
Doppler search coverage	−2000 to +2000 Hz
Robustness grid	Speed 10:5:40 m/s; $\|\alpha_1\| = 0.05{:}0.05{:}0.35$ (49 cells)
Independent repetitions	30 noise seeds, 50 snapshots per seed and condition
Receiver comparators	No cancellation; single-reference LS; tuned one-tap NLMS; three-template ECA-like

Notes: Communication and sensing use different channel and receiver assumptions. The sensing model assumes a measured reference-channel waveform; physical RSU synchronization and PSSCH reconstruction have not been demonstrated. Numerical MCS index, SCI configuration, RIV and complete PSFCH behavior are not established by the archived physical-layer audit. The 0.5-ms waveform duration is distinct from the 100-ms packet-update interval.

4. Simulation Setup and Evaluation Methodology

The NR-V2X physical-layer communication evaluation, the reference-aided bistatic sensing receiver evaluation, and the isolated-path fractional-delay/CRLB benchmark are three distinct experiments. Table 3 explicitly identifies the settings and statistical populations behind the result figures. The communication setup reports 11 SNR points and 100 SL-SCH block outcomes at each point; because it does not measure an end-to-end vehicle-message delivery process, its pooled 96.64% success must not be called packet delivery ratio (PDR). PSSCH has QPSK modulation and a stored code-rate target of 308/1024; the archive provides 1128-bit TBS, four DM-RS positions, and two groups of ten PRBs. The stored audit does not independently establish the numerical MCS index, SCI variant or RIV; these values are therefore not claimed.

Table 3. Experimental configurations, observation populations, and scope of the reported results.

Experiment and Varied Conditions	Observations and Interpretation
Separate NR-V2X PC5 communication decoding experiment; 11 SNR points	100 SL-SCH blocks per SNR point (1100 total); block-success rate and BLER, not application-layer PDR
Direct-path cancellation response for an illustrative bistatic observation	Single representative correlation trace; suppression and echo loss quantified by the matched receiver experiment, not by the plot
Nominal moving-target bistatic sensing; target speed 20 m/s, fixed trajectory	30 independent noise seeds, 50 consecutive packets per seed (1500 observations); repeated packets share a trajectory
Sensitivity to seven target speeds (10–40 m/s) and seven reflection coefficients (0.05–0.35)	49 speed–reflection cells; each cell pools 30 noise seeds × 50 packets; other modeled conditions held at their specified settings
Matched nominal receiver comparison: no cancellation, LS, tuned NLMS, and three-template ECA-like cancellation	Identical nominal packet/seed population for each receiver (30 seeds × 50 packets); receiver methods compared on matched observations
Separate isolated-path fractional-delay estimation across six SNR points and four prescribed delays	Ten noise trials per delay/SNR combination (40 trials per SNR); conditional single-path CRLB, not full bistatic receiver performance
Simulated dual-channel RSU sensing under six reference-quality or synchronization conditions	30 independent noise seeds × 50 consecutive packets per condition; isolates reference-impairment sensitivity

Notes: Independent noise seeds do not constitute independently randomized vehicle trajectories or road geometries. Communication, full bistatic sensing, and isolated-path delay-estimation results are generated under distinct experimental configurations and should not be pooled as a single operating condition.

The sensing study uses $\mathbf{p}_T = [0, 0, 1.5]$ m, $\mathbf{p}_R = [200, 0, 6]$ m and $\mathbf{p}_q(0) = [80, 80, 1.5]$ m. The direct-path baseline is 200.0506 m; the reflected path is computed from the same three-dimensional coordinates, rather than mixing the earlier static-test lengths. The nominal speed is 20 m/s, $|\alpha_0| = 1$, $|\alpha_1| = 0.35$, surveillance SNR 20 dB and reference SNR 30 dB. The 50 snapshots from 0 to 4.9 s share one trajectory per seed. The experiment varies independent noise seeds (30 per condition), not independently sampled road layouts. The 49-cell robustness study varies speed 10–40 m/s and reflection magnitude 0.05–0.35. Timing

comparisons are measured MATLAB receiver processing times, not radio propagation time, network latency or hardware real-time throughput.

For packet errors $e_{s,k}$ in seed s and packet k, pooled RMSE and mean absolute error are

$$R_{\text{pool}} = \sqrt{\frac{1}{SK}\sum_{s=1}^{S}\sum_{k=1}^{K} e_{s,k}^2}, \qquad \text{MAE} = \frac{1}{SK}\sum_{s,k}|e_{s,k}|. \tag{8}$$

The mean signed error is $(SK)^{-1}\sum_{s,k} e_{s,k}$ and is not MAE. Seed-level $R_s = \sqrt{K^{-1}\sum_k e_{s,k}^2}$ provides uncertainty computed across $S = 30$ independent noise realizations using $\bar{R} \pm t_{0.975,S-1}s_R/\sqrt{S}$. For LS, $\bar{R} = 0.545774$ m, $s_R = 0.005528$ m and the 95% confidence interval is 0.543710–0.547838 m. Within-seed packets are correlated through a shared target trajectory and must not be counted as independent driving experiments. The geometry and SNR assumptions do not establish practical road coverage or interference robustness.

5. Results and Discussion

5.1. Separate PC5 Communication Experiment

The stored eleven-SNR-point communication run reports SL-SCH block-success and BLER, rather than end-to-end application PDR. The aggregate successful-block fraction is 96.64% and the complementary BLER is 3.36%. These outcomes are conditional on the saved TDL-A30 and perfect-channel-estimation assumptions. The SNR-dependent curves in Figure 3 illustrate how decoding success and errors complement each other as the receiver operating point changes. Each point is based on 100 decoded blocks, so the pooled 96.64% average should be interpreted as a descriptive summary of the sampled SNR grid, not a traffic-weighted network reliability guarantee. In particular, the communication experiment does not establish the effect of repeated retransmissions, scheduling collisions, interference from other transmitters or application-layer packet delivery. Figure 3 presents per-SNR values and the per-point trial count; it does not demonstrate general standards compliance.

5.2. Direct-Path Cancellation and Receiver Comparison

A direct path dominates the weak target echo in the nominal reference-aided RSU model. Figure 4 is an illustrative archived correlation plot; the underlying common-amplitude waveform samples are not available in the archived numerical output, so quantitative cancellation depth must be drawn from the matched receiver table rather than inferred from separately normalized peaks. Direct suppression is measured as a simulation proxy, not a laboratory calibration. Conventional single-reference LS achieves 21.93 dB median suppression and 0.196 dB median desired-echo projection loss. Table 4 compares four implementations on identical packet/seed conditions. LS and tuned NLMS produce very similar nominal RMSE; the restricted three-template ECA-like implementation should not be interpreted as a universal best or worst ECA benchmark. The no-cancellation diagnostic often selects peaks near search boundaries (46% of packets), explaining why it is a diagnostic rather than a competitive tuned receiver. Physically, the stronger direct return and its correlation sidelobes obscure a weaker reflected path; cancellation changes the delay-search landscape, but its 21.93 dB suppression also entails a measurable 0.196 dB desired-echo loss. The residual error is therefore not simply a function of suppression depth. Notably, the 0.5458 m LS and 0.5457 m NLMS RMSEs differ by only 0.0001 m, so these observations support the effectiveness of cancellation in the defined scenario, not the superiority of LS over adaptive methods. The 4.03 ms LS and 6.54 ms NLMS receiver times are platform-dependent processing observations rather than end-to-end latency.

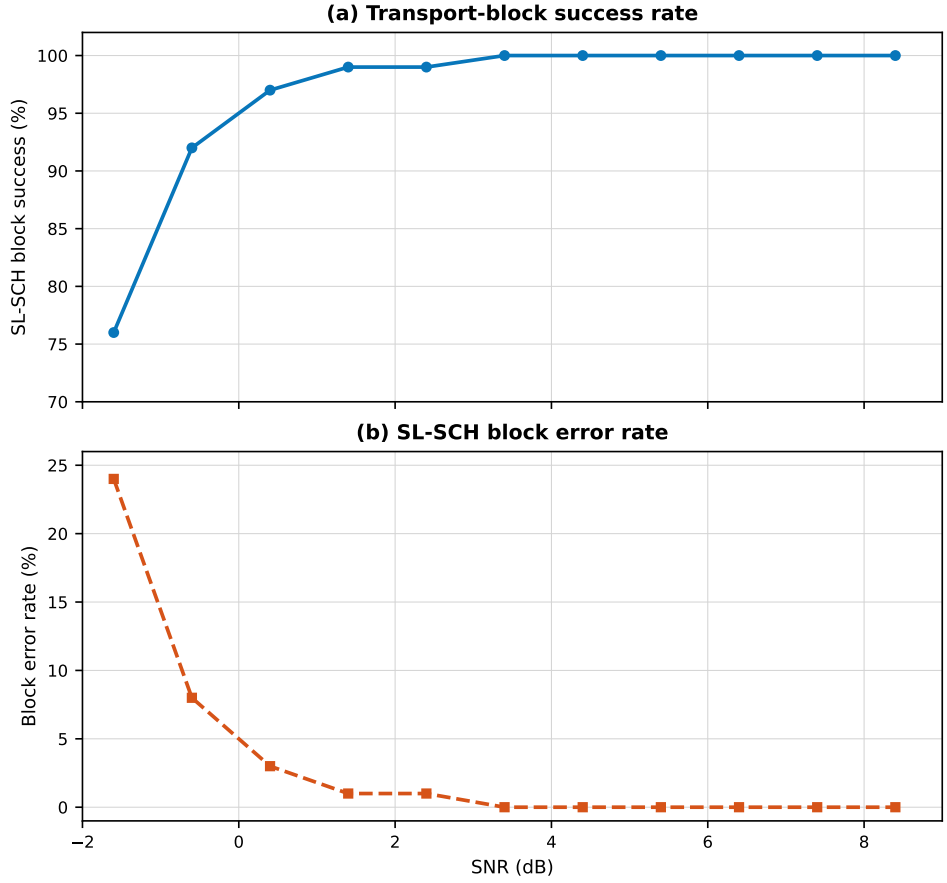


Figure 3. SL-SCH transport-block success and BLER versus SNR, 100 decoded blocks per each of 11 SNR points (separate PC5 communication experiment); success is not end-to-end packet delivery ratio.

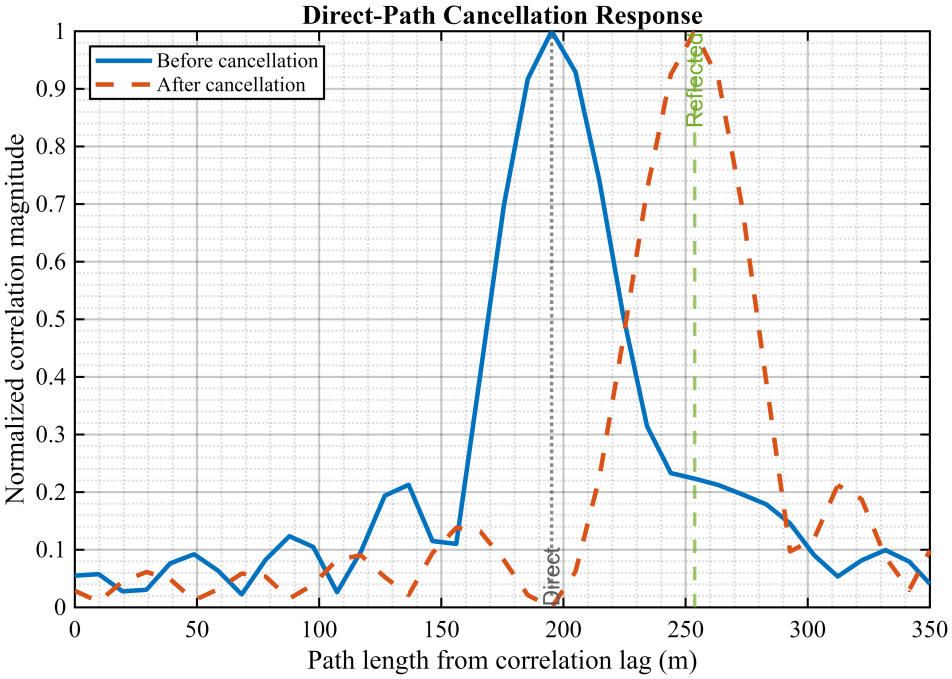


Figure 4. Illustrative archived direct-path cancellation correlation response. The displayed trace is not used to estimate suppression depth; quantitative matched-population suppression and desired-echo projection loss are reported in Table 4.

Table 4. Nominal passive-reference receiver comparison from 30 independent noise seeds and 50 packets per seed (1500 packet observations per method).

Receiver	RMSE (m)	MAE (m)	Supp. (dB)	Echo Loss (dB)	Time (ms)	Cancel. Cost
No cancellation	27.0201	20.0011	–	–	5.58	–
Single-ref. LS	0.5458	0.5002	21.93	0.196	4.03	$O(N)$
Tuned NLMS	0.5457	0.4921	21.72	0.192	6.54	$O(N)$
Three-template ECA-like	1.9806	1.6368	20.04	0.302	4.22	$O(NK^2 + K^3)$

Notes: RMSE and MAE are pooled excess-path metrics. Suppression and echo losses are simulation-derived proxies; time is the median MATLAB receiver runtime per packet (platform dependent), not over-the-air delay. Computational-order expressions represent additional cancellation arithmetic only, excluding waveform correlation, delay search, and synchronization; N is the sample count and $K = 3$ for the restricted ECA-like subspace. The no-cancellation diagnostic has frequent search-edge selections and is not an optimized competitor. The tuned NLMS and LS nominal accuracies are statistically indistinguishable in the available paired seed-level comparison.

5.3. Nominal Tracking and Speed–Reflection Robustness

In the nominal reference-aided bistatic sensing experiment, the pooled single-reference LS excess-path RMSE is 0.5458 m, MAE is 0.5002 m and mean signed error is 0.0237 m. The revised figure depicts a single representative trajectory and must not be mistaken for a display of 30 independent geometry realizations. Figure 5 shows the packet-level track, while Figure 6 reports 49 conditions with 30 noise seeds and 50 samples per seed. The pooled heatmap RMSE ranges from 0.4058 to 0.6429 m. The sensitivity experiment and nominal receiver comparison use the stated common evaluation design; older preliminary curves obtained under different settings are not included in these pooled results. The representative trajectory in Figure 5 provides a time-domain illustration of tracking against changing bistatic geometry. Its deviations must be distinguished from aggregate error statistics calculated over repeated noise realizations. The heatmap in Figure 6 quantifies sensitivity over the selected target speeds and reflection magnitudes: although all 49 cells remain within the reported 0.4058–0.6429 m pooled RMSE range, this controlled grid changes neither the road geometry nor the underlying single-target interpretation. Accordingly, the heatmap is evidence for robustness within the tested simulation envelope, not for arbitrary road conditions or cluttered multi-target scenes.

5.4. Error Distributions and Receiver Ablation

The nominal empirical CDF contains 1500 packet errors per method (30 seeds times 50 samples). The no-cancellation diagnostic yields 27.0201 m pooled RMSE and 20.0011 m MAE, whereas LS yields 0.5458 m and 0.5002 m; tuned NLMS gives 0.5457 m and 0.4921 m. The percentage computed directly from these pooled RMSEs is $100(1 - 0.5458/27.0201) \simeq 97.98\%$, not the obsolete 99.52% or 99.72% derived from unmatched earlier studies. Receiver runtime per packet was 4.03 ms for LS, 6.54 ms for NLMS, 4.22 ms for the restricted ECA-like method and 5.58 ms for the no-cancellation diagnostic, as measured in the MATLAB experiment; timings depend on implementation and hardware. Figure 7 complements the scalar RMSE comparison by showing the distribution of absolute estimation errors across the matched packet observations: a lower curve at a given error threshold indicates fewer accurate estimates, while a curve reaching a high cumulative probability earlier indicates more concentrated errors. Because observations within each 50-packet sequence share the same trajectory, packet-level CDF counts must not be treated as independent road scenarios. Figure 8 summarizes the receiver-level differences, demonstrating why a no-cancellation-only comparison would be insufficient to position the method against established adaptive techniques.

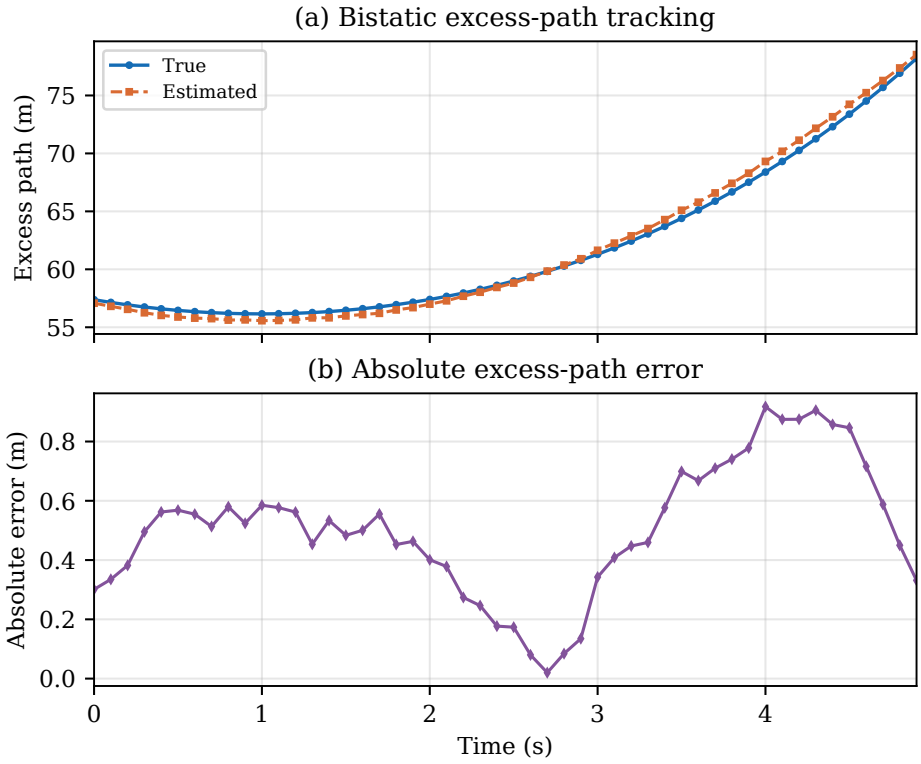


Figure 5. Representative 20 m/s moving-target excess-path tracking and error for the nominal sensing trajectory; pooled statistics across 30 independent noise seeds are reported in the text.

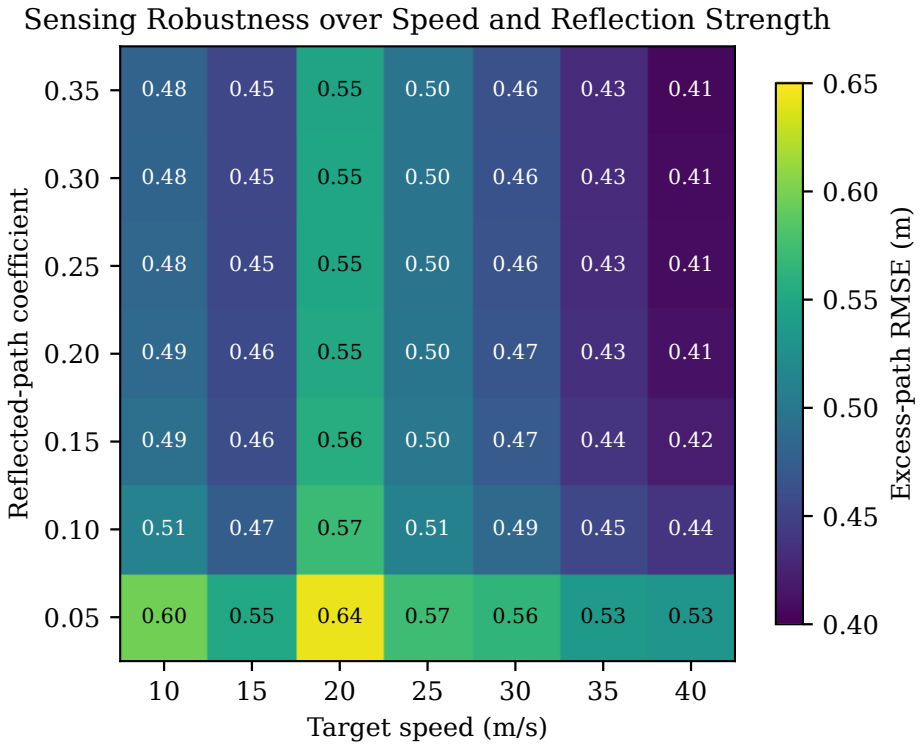


Figure 6. Pooled excess-path RMSE over speed 10–40 m/s and reflected-gain magnitude 0.05–0.35 (49 conditions; each 30 noise seeds and 50 packets per seed).

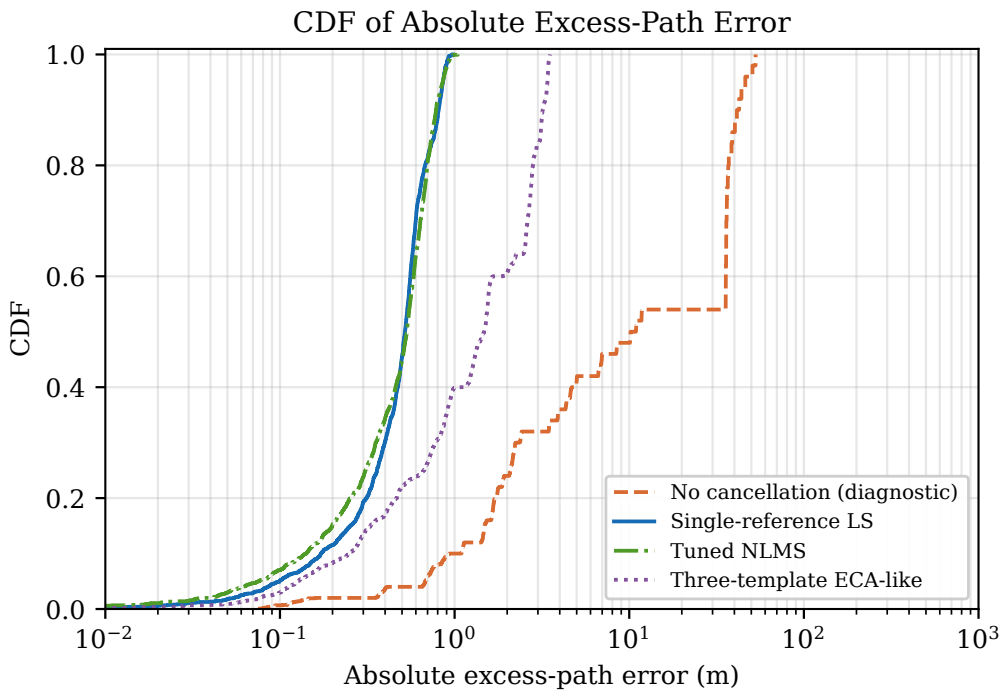


Figure 7. Empirical CDF of absolute bistatic excess-path error using four matched receivers; 1500 packet observations per receiver grouped in 30 independent noise seeds.

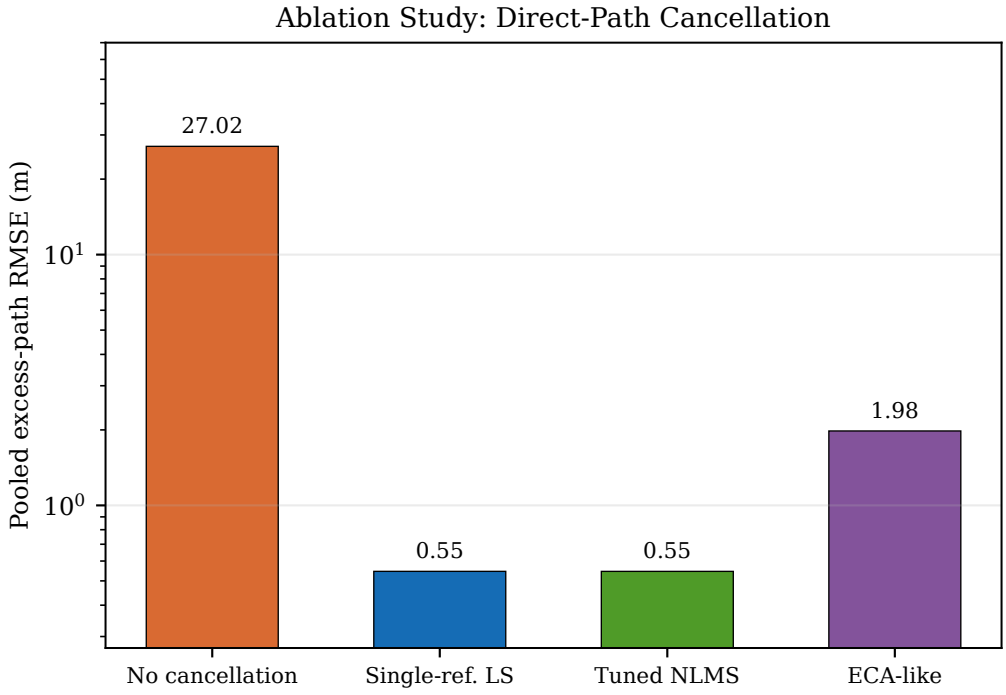


Figure 8. Matched pooled RMSE receiver ablation from the nominal matched sensing experiment, including no cancellation, conventional LS, tuned NLMS and restricted three-template ECA-like processing.

5.5. Isolated-Path Delay Precision and Conditional CRLB

At a sampling frequency of 30.72 MHz, the bistatic path per sample is about 9.7589 m, but local fractional-lag precision can be smaller under an isolated-path and sufficiently high-SNR assumption. In the separate isolated-path benchmark at 20 dB, integer-grid correlation

yields 3.0542 m RMSE, parabolic refinement 0.0509 m and bounded fractional-delay LS 0.0114 m. The conditional CRLB standard-deviation estimate is 0.0130 m. Since the quoted empirical value is numerically below this conditional bound, it should not be interpreted as proof of CRLB violation; the conditional bound, finite-sample estimator, chosen delay set and possible bias/normalization mismatch require carefully matched interpretation. The result does not imply the full receiver resolves two targets separated by less than the waveform ambiguity width as shown in Figure 9.

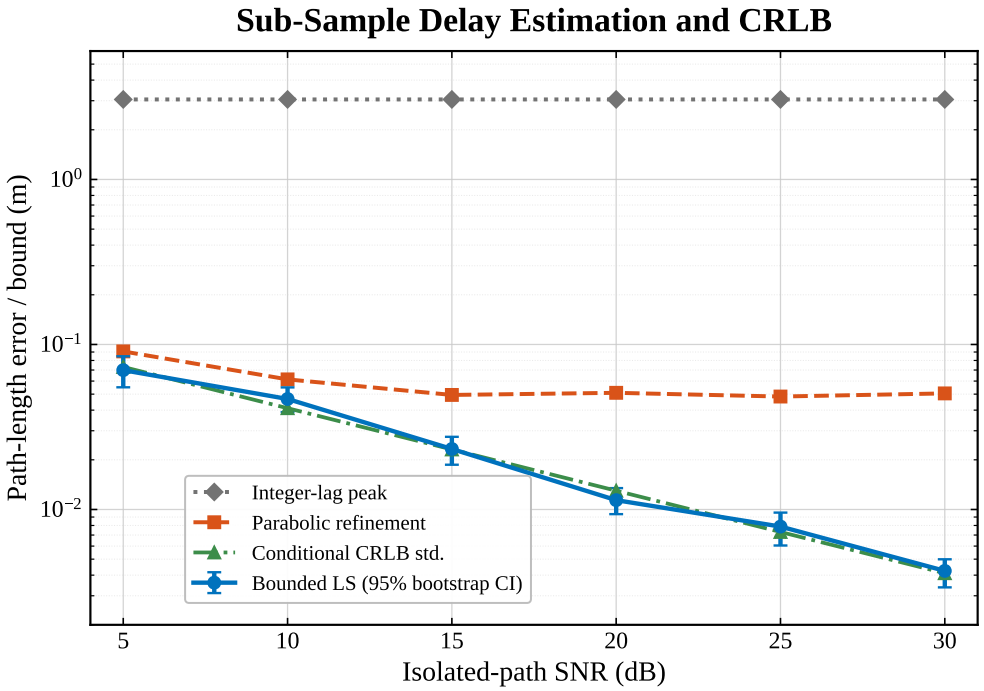


Figure 9. Isolated-path fractional-delay validation: integer-lag, parabolic and bounded LS estimation versus a conditional CRLB standard deviation; 40 noise realizations at each SNR (four delays times ten seeds). This is a separate experiment from the complete bistatic sensing model.

5.6. Reference-Channel Quality, Clutter and Synchronization

A 30-seed reference-channel sweep records nominal 0.5458 m RMSE, ideal stored-waveform reference 0.5449 m, reduced reference SNR to 20 dB 0.5812 m, added stationary clutter 2.8145 m and a 0.25-sample relative timing error 4.3055 m. A common 100 Hz offset in both channels yields 0.5456 m but does not test independent oscillator offsets. Thus the dominant measured weaknesses are clutter and inter-channel calibration. Figure 10 makes this asymmetry clear: reducing reference SNR from its nominal setting to 20 dB produces a comparatively modest change (0.5458 to 0.5812 m RMSE), whereas introducing a stationary clutter component raises the error to 2.8145 m and a 0.25-sample relative timing shift raises it to 4.3055 m. This difference emphasizes that robust reference-channel synchronization and clutter treatment are central engineering challenges for practical passive RSU sensing. Neither inter-vehicle interference nor real physical dual-channel synchronization was validated. The modeled 4.9-s trajectory is too short to establish long-term independent driving generalization or multiple-target robustness.

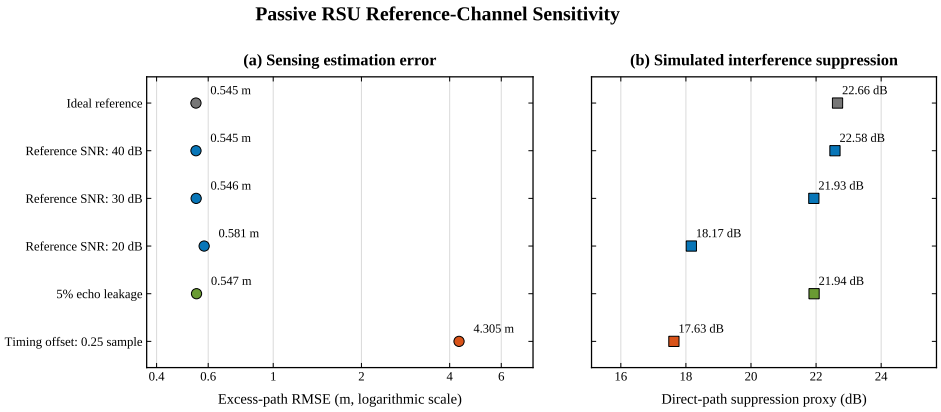


Figure 10. Reference-channel quality and calibration sensitivity from the simulated two-channel RSU model: 30 independent noise seeds, 50 snapshots per seed; suppression is a simulation proxy, not measured hardware cancellation depth.

5.7. Scope and Limitations

The reported sensing statistics are conditional on supplied synchronized PC5 reference/surveillance observations and a controlled bistatic geometry. Passive reference waveform recovery without PSCCH/PSSCH payload knowledge, independent receiver clocks and carrier errors, generalized multipath or clutter, multi-user interference, hardware sensing range and end-to-end MAC behavior remain outside validated scope. The communication receiver uses a separate channel model and its aggregate block success cannot be converted into end-to-end vehicular PDR. These explicit limitations identify concrete targets for future experiments rather than being inferred as demonstrated properties.

6. Conclusions

As connected and automated vehicles demand increasingly accurate environmental awareness, exploiting already-transmitted sidelink waveforms for infrastructure sensing offers a promising way to complement conventional V2X data exchange without introducing a dedicated sensing transmission. Motivated by this opportunity, this paper investigated a simulation-based, reference-aided NR-V2X PC5 waveform-reuse framework for RSU bistatic sensing. The sensing branch uses established direct-path LS cancellation and matched comparison receivers, with its contribution in PC5 waveform integration and explicit evaluation assumptions rather than a new cancellation principle. Under a common nominal 30-seed/50-packet condition, conventional LS obtains 0.5458 m pooled excess-path RMSE versus 0.5457 m for tuned NLMS, 1.9806 m for a restricted ECA-like receiver and 27.0201 m for a no-cancellation diagnostic. The nominal mean seed-level RMSE confidence interval is 0.5437–0.5478 m; the 49-cell speed/reflection study spans 0.4058–0.6429 m. The independent communication evaluation recorded 96.64% SL-SCH block success, not verified end-to-end PDR. Reference timing misalignment and stationary clutter substantially degrade sensing, while the limited 4.9-s common geometry and the assumed synchronized reference channels prevent claims of deployed passive sensing. Future work must validate PC5 reference acquisition, real independent-channel calibration, multi-user interference, multi-target clutter, accurate velocity extraction, and independently varied long-horizon driving scenarios.

Author Contributions: Conceptualization, M.A.; methodology, M.A.; software, M.A.; validation, M.A.; formal analysis, M.A.; investigation, M.A.; resources, S.W.K. and A.N.; writing original draft preparation, M.A.; review and editing, S.W.K. and A.N.; supervision, S.W.K. and A.N. All authors have read and agreed to the published version of the manuscript.

Funding: This research was supported by Basic Science Research Program through the National Research Foundation of Korea (NRF) funded by the Ministry of Education (RS-2021-NR060120), by the BK21 FOUR of the National Research Foundation of Korea (NRF) funded by the Ministry of Education (2120251015517), and by the NRF grant funded by the Korea government (MSIT) (RS-2022-NR069161).

Data Availability Statement: The simulation results and configuration details supporting the findings of this study are available from the corresponding author upon reasonable request.

Conflicts of Interest: The authors declare no conflicts of interest.

References

1. 3GPP. *Enhancement of 3GPP Support for V2X Scenarios*; Technical Specification Technical Report TS 22.186; 3rd Generation Partnership Project (3GPP): Sophia Antipolis, France, 2024.
2. 5G Automotive Association. *C-V2X Use Cases and Service Level Requirements, Volume I*; Technical report; 5GAA: Munich, Germany, 2025.
3. 5G Automotive Association. *5G-V2X Direct Communication Evaluation Approach*; Technical report; 5GAA: Munich, Germany, 2024.
4. 3GPP. *Architecture Enhancements for 5G System (5GS) to Support Vehicle-to-Everything (V2X) Services*; Technical Specification Technical Report TS 23.287; 3rd Generation Partnership Project (3GPP): Sophia Antipolis, France, 2024.
5. 3GPP. *Overall Description of Radio Access Network (RAN) Aspects for Vehicle-to-Everything (V2X) Based on LTE and NR*; Technical Report TR 37.985; 3rd Generation Partnership Project (3GPP): Sophia Antipolis, France, 2024.
6. Garcia, M.H.C.; Molina-Galan, A.; Boban, M.; Gozalvez, J.; Coll-Perales, B.; Sahin, T.; Kousaridas, A. A Tutorial on 5G NR V2X Communications. *IEEE Commun. Surv. Tutor.* **2021**, *23*, 1972–2026. [CrossRef]
7. Harounabadi, M.; Soleymani, D.M.; Bhadauria, S.; Leyh, M.; Roth-Mandutz, E. V2X in 3GPP Standardization: NR Sidelink in Release 16 and Beyond. *IEEE Commun. Stand. Mag.* **2021**, *5*, 12–21. [CrossRef]
8. 3GPP. *NR; Physical Channels and Modulation*; Technical Specification Technical Report TS 38.211; 3rd Generation Partnership Project (3GPP): Sophia Antipolis, France, 2024.
9. 3GPP. *NR; Multiplexing and Channel Coding*; Technical Specification Technical Report TS 38.212; 3rd Generation Partnership Project (3GPP): Sophia Antipolis, France, 2024.
10. 3GPP. *NR; Physical Layer Procedures for Control*; Technical Specification Technical Report TS 38.213; 3rd Generation Partnership Project (3GPP): Sophia Antipolis, France, 2024.
11. 3GPP. *NR; Physical Layer Procedures for Data*; Technical Specification Technical Report TS 38.214; 3rd Generation Partnership Project (3GPP): Sophia Antipolis, France, 2024.
12. Liu, F.; Cui, Y.; Masouros, C.; Xu, J.; Han, T.X.; Eldar, Y.C.; Buzzi, S. Integrated Sensing and Communications: Toward Dual-Functional Wireless Networks for 6G and Beyond. *IEEE J. Sel. Areas Commun.* **2022**, *40*, 1728–1767. [CrossRef]
13. Zhang, J.A.; Liu, F.; Masouros, C.; Heath, R.W.; Feng, Z.; Zheng, L.; Petropulu, A. An Overview of Signal Processing Techniques for Joint Communication and Radar Sensing. *IEEE J. Sel. Top. Signal Process.* **2021**, *15*, 1295–1315. [CrossRef]
14. Wei, Z.; Qu, H.; Wang, Y.; Yuan, X.; Wu, H.; Du, Y.; Han, K.; Zhang, N.; Feng, Z. Integrated Sensing and Communication Signals Toward 5G-A and 6G: A Survey. *IEEE Internet Things J.* **2023**, *10*, 11068–11092. [CrossRef]
15. Wild, T.; Grudnitsky, A.; Mandelli, S.; Henninger, M.; Guan, J.; Schaich, F. 6G Integrated Sensing and Communication: From Vision to Realization. In Proceedings of the 2023 20th European Radar Conference (EuRAD), Berlin, Germany, 20–22 September 2023; pp. 355–358. [CrossRef]
16. ITU-R. *Framework and Overall Objectives of the Future Development of IMT for 2030 and Beyond*; Technical Report Recommendation ITU-R M.2160-0; International Telecommunication Union Radiocommunication Sector: Geneva, Switzerland, 2023.
17. Kaushik, A.; Singh, R.; Dayarathna, S.; Senanayake, R.; Renzo, M.D.; Dajer, M.; Ji, H.; Kim, Y.; Sciancalepore, V.; Zappone, A.; et al. Towards Integrated Sensing and Communications for 6G: A Standardization Perspective. *IEEE Commun. Stand. Mag.* **2024**, *8*, 52–59. [CrossRef]
18. 3GPP. *Study on Integrated Sensing and Communication*; Technical Report TR 22.837, Release 19; 3rd Generation Partnership Project (3GPP): Sophia Antipolis, France, 2025.
19. 3GPP. *Study on Integrated Sensing and Communication (ISAC) for NR*; Technical Report TR 38.765, Release 20 draft; 3rd Generation Partnership Project (3GPP): Sophia Antipolis, France, 2025.
20. Colone, F.; O'Hagan, D.W.; Lombardo, P.; Baker, C.J. A Multistage Processing Algorithm for Disturbance Removal and Target Detection in Passive Bistatic Radar. *IEEE Trans. Aerosp. Electron. Syst.* **2009**, *45*, 698–722. [CrossRef]
21. Giovannetti, C.; Decarli, N.; Bartoletti, S.; Stirling-Gallacher, R.A.; Masini, B.M. Target Positioning Accuracy of V2X Sidelink Joint Communication and Sensing. *IEEE Wirel. Commun. Lett.* **2024**, *13*, 849–853. [CrossRef]

22. Decarli, N.; Bartoletti, S.; Bazzi, A.; Stirling-Gallacher, R.A.; Masini, B.M. Performance Characterization of Joint Communication and Sensing With Beyond 5G NR-V2X Sidelink. *IEEE Trans. Veh. Technol.* **2024**, *73*, 10044–10059. [CrossRef]
23. Nataraja, N.K.; Sharma, S.; Ali, K.; Bai, F.; Wang, R.; Molisch, A.F. Integrated Sensing and Communication (ISAC) for Vehicles: Bistatic Radar With 5G-NR Signals. *IEEE Trans. Veh. Technol.* **2025**, *74*, 6121–6137. [CrossRef]
24. Wypich, M.; Zielinski, T.P. Experimental Evaluation of 5G NR OFDM-Based Passive Radar Exploiting Reference, Control, and User Data. *Sensors* **2026**, *26*, 1317. [CrossRef] [PubMed]
25. 3GPP. *Study on NR Vehicle-to-Everything (V2X)*; Technical Report TR 38.885; 3rd Generation Partnership Project (3GPP): Sophia Antipolis, France, 2019.
26. Ali, Z.; Lagén, S.; Giupponi, L.; Rouil, R. 3GPP NR V2X Mode 2: Overview, Models and System-Level Evaluation. *IEEE Access* **2021**, *9*, 89554–89579. [CrossRef] [PubMed]
27. Bagheri, H.; Noor-A-Rahim, M.; Liu, Z.; Lee, H.; Pesch, D.; Moessner, K.; Xiao, P. 5G NR-V2X: Toward Connected and Cooperative Autonomous Driving. *IEEE Commun. Stand. Mag.* **2021**, *5*, 48–54. [CrossRef]
28. Coll-Perales, B.; Lucas-Estañ, M.C.; Shimizu, T.; Gozalvez, J.; Higuchi, T.; Avedisov, S.S.; Altintas, O.; Sepulcre, M. End-to-End V2X Latency Modeling and Analysis in 5G Networks. *IEEE Trans. Veh. Technol.* **2023**, *72*, 5094–5109. [CrossRef]
29. Lucas-Estañ, M.C.; Coll-Perales, B.; Shimizu, T.; Gozalvez, J.; Higuchi, T.; Avedisov, S.S.; Altintas, O.; Sepulcre, M. An Analytical Latency Model and Evaluation of the Capacity of 5G NR to Support V2X Services Using V2N2V Communications. *IEEE Trans. Veh. Technol.* **2023**, *72*, 2293–2306. [CrossRef]
30. Wang, Q.; Kakkavas, A.; Gong, X.; Stirling-Gallacher, R.A. Towards Integrated Sensing and Communications for 6G. In Proceedings of the 2022 2nd IEEE International Symposium on Joint Communications & Sensing (JC&S), Seefeld, Austria, 9–10 March 2022; pp. 1–6. [CrossRef]
31. Wen, D.; Zhou, Y.; Li, X.; Shi, Y.; Huang, K.; Letaief, K.B. A Survey on Integrated Sensing, Communication, and Computation. *IEEE Commun. Surv. Tutor.* **2025**, *27*, 3058–3098. [CrossRef]
32. Du, Z.; Liu, F.; Yuan, W.; Masouros, C.; Zhang, Z.; Xia, S.; Caire, G. Integrated Sensing and Communications for V2I Networks: Dynamic Predictive Beamforming for Extended Vehicle Targets. *IEEE Trans. Wirel. Commun.* **2023**, *22*, 3612–3627. [CrossRef]
33. Salami, D.; Hasibi, R.; Savazzi, S.; Michoel, T.; Sigg, S. Angle-Agnostic Radio Frequency Sensing Integrated Into 5G-NR. *IEEE Sens. J.* **2024**, *24*, 36099–36114. [CrossRef]

Disclaimer/Publisher's Note: The statements, opinions and data contained in all publications are solely those of the individual author(s) and contributor(s) and not of MDPI and/or the editor(s). MDPI and/or the editor(s) disclaim responsibility for any injury to people or property resulting from any ideas, methods, instructions or products referred to in the content.